Electronic Journal of Structural Engineering

Original Article

Cite this: DOI:10.56748/ejse.23544

Received Date:02 November 2023
Accepted Date:21 December 2023

1443-9255
https://ejsei.com/ejse

Study on the influence of roof load combination on deformation control of shallow buried tunnel section

Lin ZHANG[a]*
The 5th Engineering Co., Ltd., China Railway Construction Bridge Engineering Bureau Group, Sichuan, Chengdu 610500
*Corresponding author: 2696220756@qq.com

Abstract

The shallow buried section at the exit of a tunnel in southwestern Sichuan Province is affected by the combination of loads on the roof of the tunnel, resulting in deformation phenomena that affect the safety and stability of tunnel construction. Based on the theory of elastic-plastic mechanics, combined with finite element numerical simulation, the article analyzes the stress distribution characteristics, plastic zone development, and deformation characteristics of the surrounding rock of this tunnel section under different load combinations, exposes the influence of load combinations on the deformation of the tunnel, and puts forward a solution for the deformation of the surrounding rock during this tunnel construction. The results show that the stress at the foot of the tunnel is more concentrated in the early stage of tunnel excavation, and the stress at the foot of the tunnel produces a maximum value of stress, which gradually decreases from the foot of the arch to the top of the arch. The load combination has no significant effect on the stress concentration areas but will significantly increase the stress values at the foot of the arch. After excavation, the plastic zone of peripheral rock appears at the location of the side wall. With the construction of the primary support, the primary support bears the lateral pressure of the peripheral rock and transmits the pressure of the peripheral rock to the foot of the tunnel primary support, and the plastic zone is then transferred to the peripheral rock at the bottom of the foot of the primary support. The greatest deformation of the tunnel surrounding rock occurs at the roof or bottom of the tunnel, and the amount of displacement increases continuously with the increase of load. For the deformation characteristics of the tunnel surrounding rock after tunnel excavation and after various types of loads are applied during the construction process, the deformation control measures to be taken under each working condition are proposed, and these measures have a positive effect on the stability of the tunnel structure.

Keywords

Tunnel, Load combination, Elastoplastic mechanics, Numerical simulation, Deformation control

1. Introduction

With the rapid development of China's transportation construction, transportation routes continue to extend to mountainous areas, making the tunnel project gradually increase. During the construction of tunnels, there are often more temporary structures, and terrain conditions ease of use, and other factors make this part of the load often distributed on top of the tunnel or around it, which has a great impact on the construction of new tunnels and the safety of the structure (Liu.,2022), especially for the construction of shallow buried tunnel sections.

Tunnel excavation causes stress redistribution in the surrounding rock near the excavation face, resulting in plastic deformation zones of varying degrees in various parts of the tunnel (Xu et al.,2023; Gao et al.,2022). For the deformation characterization of rock bodies under excavation or loading, elastoplastic mechanics methods based on the Mohr-Coulomb principal model and Drucker-Prager principal model are often used (Cao et al.,2021; Gu.,2022; Gao et al.,2020), and combined with the rock body strain softening model, to truly reflect the deformation of the rock body (Zgur et al.,2021; Xu et al.,2022). The deformation control of surrounding rock is one of the important factors to ensure the stability of tunnel structure, to achieve this control goal, many scholars at home and abroad have carried out in-depth research for this. Lunardi (Lunardi.,2008) and Giovanni (Giovanni.,2016) analyzed the full-section excavation and boring methods for tunnels in complex engineering geological conditions and summarized the important connection between the stability of the palisade the structural stability of the tunnel, and the feasibility of full-section excavation. Xingwei Zhang (Zhang et al.,2022) analyzed the deformation of weak geotechnical bodies in shallow buried tunnels and proposed different work optimization methods to cope with the settlement problem. Wang Jinming (Wang et al.,2008) and others proposed disposal measures such as optimizing the chemical method and increasing the reserved deformation based on the on-site monitoring data and damage characterization of tunnels under construction. Guo Xiaolong (Guo et al.,2022) put forward the control measures of soft rock deformation of Chenglan Railway through mathematical statistics and optimization analysis method, focusing on "active control, optimization process, timely support". Tang Xi (Tang.,2023) studied the surface settlement characteristics of subway tunnels underneath existing elevated intervals, and the study showed that the range of significant impacts is about four times the tunnel span. Zhu Yiqiao (Zhu.,2022) studied the impact of pit excavation on existing railroad tunnels in soft soil areas and found that soft soil pit excavation next to the existing railroad will cause significant impacts, unreasonable construction will aggravate the degree of impacts, the use of "zonal excavation, the installation of additional protective structures" can effectively reduce the impact on the existing railroad. To obtain reasonable design parameters when crossing the existing tunnels nearby, the ground displacement calculation method considering the coexistence of hydraulic expansion and infiltration and diffusion modes of the slurry was introduced, and a coupled calculation model of the deformation response of the grouting construction and the neighboring existing tunnels was established (Jiang et al.,2024). For the construction deformation characteristics of loess tunnels, the deformation law and mechanical characteristics of large section loess tunnel cutter shield construction under the influence of different burial depths are proposed (Jiang et al.,2023). The granite intrusion contact zone has a significant impact on the stability of the tunnel, and the deformation instability section is in the intrusion contact zone of granite and sandstone (Zhang et al.,2023). When investigating the effect of anisotropic stress conditions on the deformation and sequential excavation performance of tunnels in a rock mass, it was found that the yield zone becomes asymmetric as the stresses become anisotropic (Anuj et al.,2023).

In this paper, based on analytical methods and numerical simulation, the deformation characteristics of the peripheral rock in the shallow buried section at the exit of a tunnel in southwest Sichuan were investigated under the action of load combination. According to the stress characteristics, plastic zone, and deformation of the tunnel surrounding rock, the control measures for the stability of the surrounding rock under each working condition are proposed. The relevant research results can provide favorable conditions for engineers and technicians to select suitable engineering measures and provide certain references for the construction of similar engineering projects.

2. Project Profile and Load Combination

Sichuan Province, southwest of tunnel K17 + 020 mileage for the tunnel exit shallow buried section, the tunnel depth of about 24.80m, the left and right line spacing of about 25.20m. The surrounding rock of this section of the tunnel is broken, mainly composed of block rubble from artificial accumulation and avalanche accumulation, loose to slightly dense. The situation inside the tunnel is shown in Figure 1.

Fig.1 Engineering geology of the left and right holes of the tunnel

During tunnel construction, due to site constraints, it is proposed to set up a concrete mixing plant and silo at the top of the tunnel and to consider the traffic load of concrete transportation tankers and ordinary vehicles. Figure 2 shows the structural layout of the tunnel at K17+020 and the location of the mixing station, silo, vehicle loading, and other settings at the top of the tunnel.

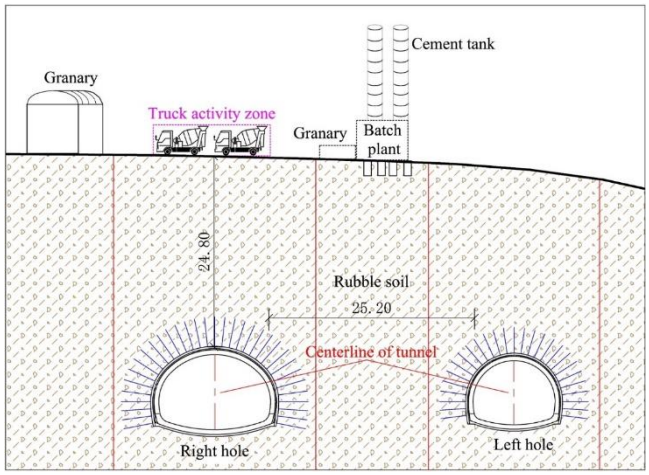

Fig.2 Layout of tunnel structure and ancillary facilities

According to the site conditions, the permanent load of the tunnel includes the self-weight of the structure and surrounding rock, the self-weight of the mixing plant and silo, the variable load includes the concrete transportation tanker on the roof of the cave and ordinary vehicles, and other variable loads and incidental loads may not be considered.

Permanent load: The self-weight of the structure is automatically considered after adding the acceleration of gravity, which is taken as g = 9.80 m/s2. The mixing plant loads are applied to the corresponding positions at the top of the strata through nodal loads, the total weight of the two mixing plants is 220T, and the permanent load sub-coefficient is taken as 1.2, which is converted to a load of:

$$F = -1.2 \times 220 \times 1000 \times 10 = -2.64 \times 10^6 N \quad (1)$$

Silo loads are considered at 10 m width and 2.5 m thickness, which translates to a load of:

$$F = -1.2 \times 10 \times 2.5 \times 20 \times 1000 = -0.6 \times 10^6 N \quad (2)$$

Live load: Cave roof car load is considered according to the most unfavorable action position, acting on the right cave roof within 10m, the live load sub-coefficient is taken as 1.4, and then through the node force is applied to the corresponding position at the top of the stratum, the total weight of the car is designed according to 200T, and it is arranged in the position of the right cave roof, which is converted into the load as:

$$F = -1.4 \times 200 \times 1000 \times 10 = -2.8 \times 10^6 N \quad (3)$$

Ordinary lane loads are converted to loads using highway-class-I lane loads (uniform loads of 10.5 kN/m):

$$q = -1.4 \times 10.5 \times 1000 = -1.47 \times 10^4 N/m$$
$$F = -1.4 \times 296 \times 1000 = -0.42 \times 10^6 N \quad (4)$$

3. Analysis of elastic-plastic mechanics of surrounding rock deformation under load effect

Adopting the Drucker-Prager principal model can accurately describe the plasticity characteristics of rock materials under loading conditions. In this study, the Drucker-Prager principal model is used as the basis (Wang et al.,2015), combined with the strain softening characteristics of the rock body for analytical solution of the surrounding rock deformation.

The plastic yield function is as follows:

$$\Phi(\sigma, c) = \sqrt{J_2(s(\sigma))} + \eta p(\sigma) - \xi c \quad (5)$$

where: $\boldsymbol{p = 1/3tr[\sigma]}$ is the hydrostatic pressure; $\boldsymbol{J_2 = 1/2s:s}$ is the second invariant of the bias stress; $\boldsymbol{s = \sigma - p(\sigma)I}$ is the bias stress tensor, $\boldsymbol{I = \delta_{ij} e_i \otimes e_j, i, j = 1, 2, 3; \eta, \xi}$ is a variable related to the strength parameter of the material; and is the cohesive force.

$\boldsymbol{\eta}$、$\boldsymbol{\xi}$ is the variable associated with the angle of internal friction of the material:

$$\eta = \frac{6 \sin \phi(k)}{\sqrt{3}[3 - \sin \phi(k)]}, \quad \xi = \frac{6 \cos \phi(k)}{\sqrt{3}[3 - \sin \phi(k)]} \quad (6)$$

The plastic potential function under the uncorrelated flow criterion is expressed as:

$$\Psi(\sigma, c) = \sqrt{J_2(s(\sigma))} + \eta' p(\sigma) \quad (7)$$

where: $\boldsymbol{\eta'}$ is a parameter related to the shear expansion angle φ,

The non-associative flow law for solving plastic strains is as follows:

$$\bar{\varepsilon}^p = \lambda N = \lambda \frac{\partial \psi}{\partial \sigma} = \frac{1}{2\sqrt{J_2(s)}} S + \frac{\eta'}{3} I \quad (8)$$

Where λneeds to satisfy the loading and unloading criteria:

$$\lambda \geq 0, \ \Phi(\sigma, c) \leq 0, \ \lambda \Phi(\sigma, c) = 0 \quad (9)$$

where: λ is the plasticity factor; N is the flow vector.

In this study, it is assumed that the mechanical parameter c, ϕ is a nonlinear function of the equivalent plastic strain (Zhang et al.,2008), which varies by the conventional strain softening model:

$$\bar{\varepsilon}^p = \frac{\sqrt{2}}{3} \sqrt{(\varepsilon_{p1} - \varepsilon_{p2})^2 + (\varepsilon_{p2} - \varepsilon_{p3})^2 + (\varepsilon_{p3} - \varepsilon_{p1})^2} \quad (10)$$

where: $\boldsymbol{\varepsilon_{p1}, \varepsilon_{p2}, \varepsilon_{p3}}$ is the main plastic strain component.

The Newton-Raphson method and Arc-Length method are used for joint iterative solution (referred to as NR-AL method) (Wang.,2014), and the solution process is as follows:

The NR method is first performed to solve for the load step displacements, and the $(n+1)^{st}$ load step is initialized $(k = 0)$ with initial values of displacements and incremental load factors:

$$\boldsymbol{u_{n+1}^0 = u_n, \ r^0 = \lambda_{n+1} \bar{f}^{ext} - \bar{f}^{int}(u_n)} \quad (11)$$

The overall stiffness matrix is used to solve for the incremental iterative displacement $\boldsymbol{\delta u^k}$ at step $k = k + 1$:

$$\boldsymbol{K_T \delta u^k = r^{k-1}} \quad (12)$$

Solve for the incremental displacement Δu_{n+1}^k and the total displacement u_{n+1}^k :

$$\Delta u_{n+1}^k = \Delta u_{n+1}^{k-1} + \delta u^k, \ u_{n+1}^k = u_{n+1}^{k-1} + \delta u^k \quad (13)$$

Update the residual force vector to determine convergence:

$$r^k = f^{int}{}_{n+1}^{k} {}_{n+1}^{-k} {}^{ext} \quad (14)$$

Convergence is achieved when: $\|r\| / \|f^{ext}\| \leq \upsilon_{tol}$ (υ_{tol} is the tolerance error).

Initialize the positive definiteness of the tangent stiffness and initiate the arc length method of solving before the positive stiffness is about to end. Initialize the parameters:

$$\boldsymbol{u_{n+1}^0 = u_n, \ \lambda_{n+1}^0 = \lambda_n, \ r^0 = \lambda_n \bar{f}^{ext} - \bar{f}^{int}(u_n)} \quad (15)$$

Solve for tangent displacement and iterative displacement δu^*:

$$\delta \bar{u} = K_T^{-1} \bar{f}^{ext}, \ \delta u^* = K_T^{-1} r^{k-1} \quad (16)$$

Then the incremental iteration loading factor can be solved by the following equation:

$$a_1\delta(\lambda^k)^2 + a_2\delta\lambda^k + a_3 = 0 \quad (17)$$

Where:$a_1 = \delta\bar{u}^T\delta\bar{u}, a_2 = 2(\Delta u^{k-1} + \delta u^*)^T\delta\bar{u}, a_3 = (\Delta u^{k-1} + \delta u^*)^T(\Delta u^{k-1} + \delta u^*) - l^2$.

The total displacement and total load factor are solved by the updated incremental displacement and incremental load factor:

$$\boldsymbol{u_{n+1}^k = u_{n+1}^{k-1} + \delta u^k,\ \lambda_{n+1}^k = \lambda_{n+1}^{k-1} + \delta\lambda^k} \quad (18)$$

The residual force vector is updated according to Eq. (14) and calculated until convergence.

4. Simulation of Deformation Characteristics of Shallow Buried Sections of Tunnels

4.1 Calculation model, parameters, and working conditions.

Based on the above elastoplastic mechanical analysis of the surrounding rock deformation, the solution program of the Drucker-Prager principal model was compiled in C++, and its correctness was verified. Based on the programming language, the finite element software ANSYS is used to realize the simulation of the deformation characteristics of the shallow buried section of this tunnel, assuming that the concrete and gravel soil materials are continuous homogeneous bodies. At the same time, according to the calculation theory of the tunnel stratum structure analysis method, the interlayer misalignment between the tunnel structure and the surrounding rock is ignored, the horizontal displacement is constrained by the left and right-side boundaries of the stratum structure, and the vertical displacement is constrained by the bottom of the stratum structure.

In this project, the plane strain model is used, and the constructed stratigraphic model is 150 m wide and 80 m high, and the plane strain model with plane183 units is used to simulate the tunnel lining, initial support, grouted surroundings, and non-grouted surroundings respectively. It is assumed that the tunnel surrounding the rock is homogeneous and conforms to the simplified model of continuous medium material, and the interlayer misalignment between the initial support and the tunnel surrounding the rock is ignored. The initial support model is an average model of concrete, steel frame, and reserved deformation, and the equivalent stiffness is used to simulate the tunnel's initial support equivalently. The model and loads are shown in Figure 3 and Figure 4.

The materials involved in the tunnel calculation include initial support concrete, tunnel surrounding rock (grouting), and tunnel surrounding rock (non-grouting), and the second lining force is not considered for the time being. The physical and mechanical parameters of each material are shown in Table 1.

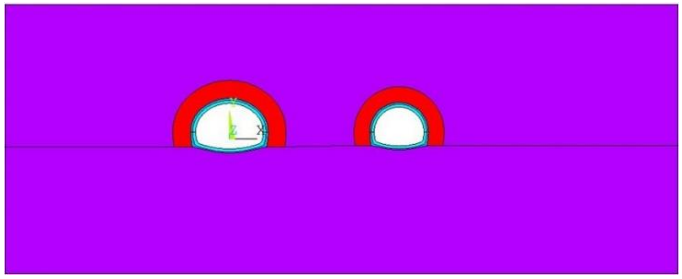

Fig.3 Composite Lined Tunnel Structural Calculation Model

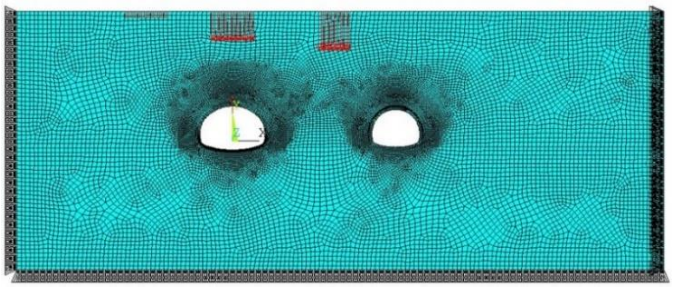

Fig.4 Structural computational modeling, cell division, and boundary conditions for composite lined tunnels

Table 1 Physical and mechanical parameters of the surrounding rock and lining structure.

Material	Γ (kN/m³)	E (GPa)	μ	C (MPa)	Φ (°)	Strength design value (MPa)
C20 concrete	25	25.5	0.17	0.5	40	9.60
Steel section	78.5	2.1	0.33	—	—	—
Rubble soil (grouted)	21	0.4	0.25	0.2	35	3.85
Rubble soil (non-grouted)	19	0.2	0.30	0.13	30	3.20

According to the load application during tunnel excavation, this analysis is divided into five working conditions. Details of the load combinations for each working condition are shown in Table 2.

Table 2 Combination of loads on the roof of the cave under each working condition

Working condition	Load combination
A	No initial support and no load
B	With initial support and no load
C	Initial support + silo + general vehicles
D	Initial support + silo + mixing plant
E	Initial support + silo + mixing plant + concrete transportation tanker

4.2 Characteristics of stress distribution under different working conditions

Tunnel excavation often causes a stress redistribution phenomenon in the tunnel rock body, which is manifested in the stress deflection around the wall, the tangential stress close to the wall reaches the maximum, while the radial stress is the minimum, and gradually recovers to the original state of the ground stress in the direction away from the wall. The state of stress distribution for each working condition A, B, C, D, and E after tunnel excavation is shown in Fig. 5 (a, b, c, d, and e). The great value of equivalent force under each working condition occurs in the region of the arch foot, gradually decreasing from the arch foot to the top of the arch, and the equivalent force of the arch foot of the right hole is greater than that of the arch foot of the left hole.

The stress distribution shows that in the case of one-time tunnel excavation, with no load on the roof of the tunnel and no construction of the initial support (Fig. 5a), the great value of the equivalent stress of the arch foot of the right tunnel is as high as 3.74MPa, which is larger than the design value of the natural strength of the tunnel surrounding rock (crushed rock soil), which is not conducive to the safety of the tunnel. After applying the initial support (Fig. 5b), due to the influence of the support structure, the equivalent stress increases, and there is a great value of the equivalent stress of 8.39MPa at the arch foot of the right hole, which is lower than the strength design value of the support concrete, and the support structure is stable. When the silo and ordinary vehicle loads are installed on the roof of the cave (Fig 5c), the stability of the tunnel structure is less affected by this part of the load because it is small, and it only slightly increases the surrounding rock stresses. The installation of the mixing plant at the roof (Fig. 5d) greatly increases the load level, and the maximum equivalent stress in the foot of the arch area reaches 9.09 MPa, which is only slightly lower than the design value of the strength of the tunnel support concrete. When the load of the concrete transportation tanker (Fig. 5e) is applied at the same time, so that the equivalent stress value reaches 9.59MPa, currently the support structure also reaches the strength limit.

4.3 Distribution characteristics of the plastic zone under different working conditions

The development of plastic zones is a necessary and insufficient condition for deformation and damage to occur in the surrounding rock, and often the development of plastic zones reveals the stresses in the weak internal parts of the surrounding rock. In this paper, the development of a plastic zone for each condition during tunnel excavation and roof loading is shown in Figure. 6 (a, b, c, d, e). Figure 6a shows the development of the plastic zone in the surrounding rock under the condition of one-time excavation without load and initial support (Condition A).

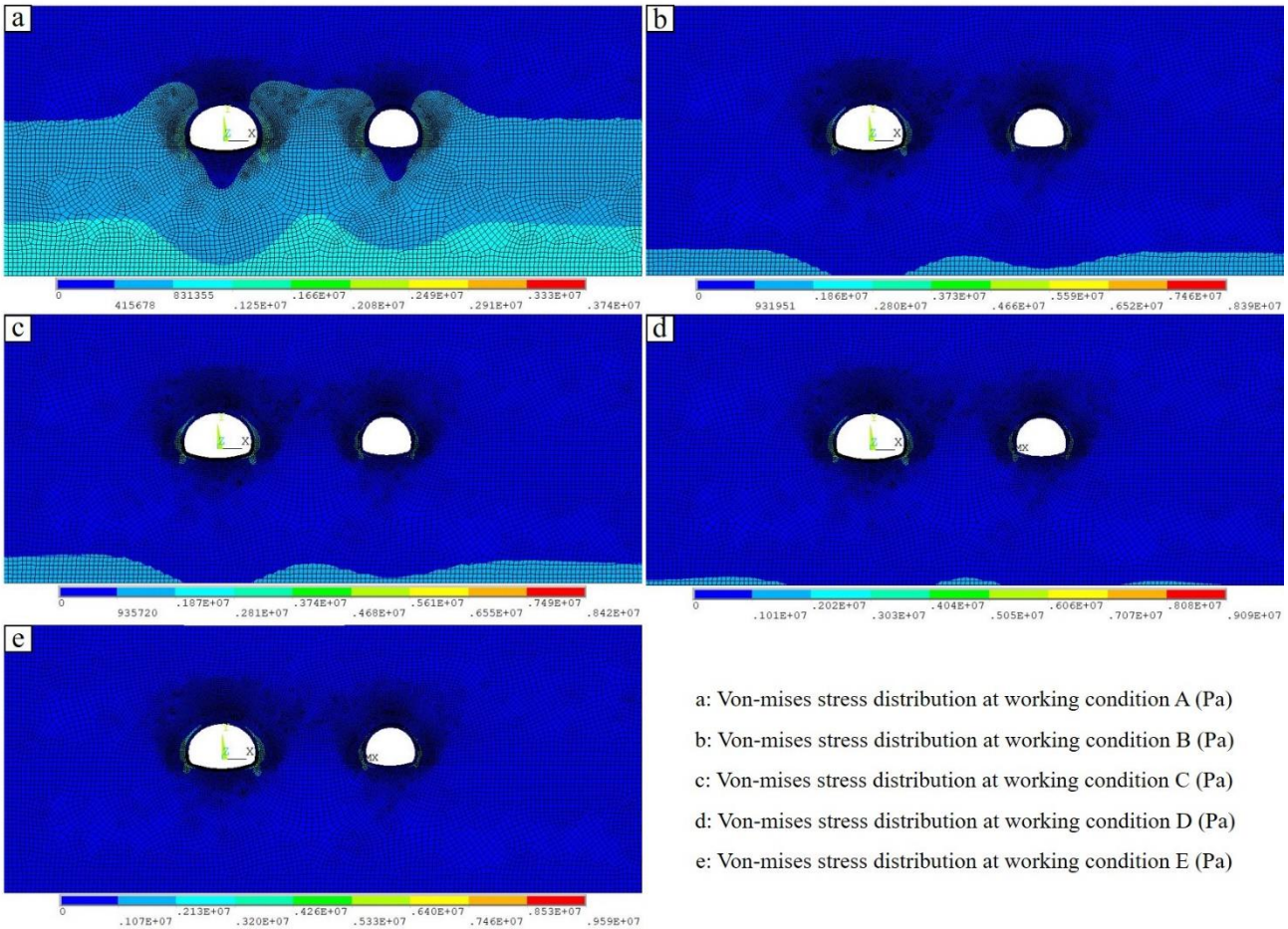

Fig.5 Von-mises stress distribution at each working condition

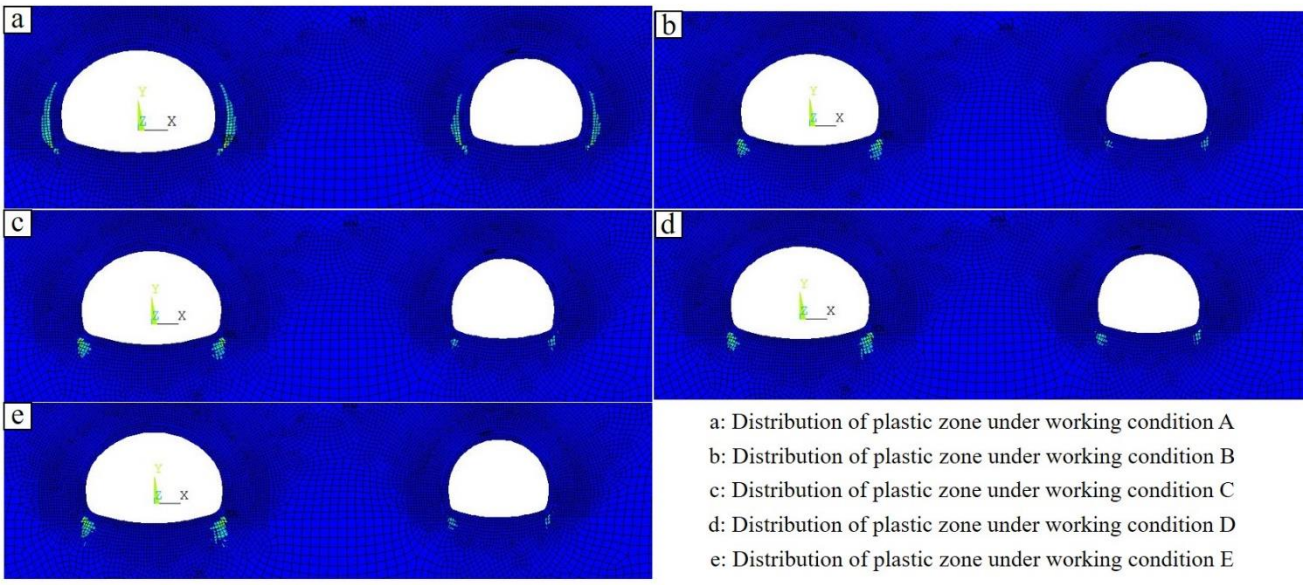

Fig.6 Distribution of plastic zone under each working condition

In this condition, the surrounding rock of the left and right sidewalls of the tunnel shows a penetrating plastic zone, and the tunnel structure is extremely unstable. The step method of excavation is used in actual construction, and the tunnel structure is relatively stable as stress redistribution occurs in the surrounding rock around the tunnel during tunnel excavation. After applying the initial support (Condition B), the development of the plastic zone is effectively suppressed, only part of the surrounding rock at the foot of the tunnel appeared in the plastic zone, the plastic area is small, the tunnel structure is stable, but the surrounding rock at the foot of the arch is more concentrated stress. With the successive application of ordinary vehicle loads and loads from the silo on the roof of the tunnel (Condition C), mixing station (Condition D), and concrete transportation tanker (Condition E), the plastic zone is continuously enlarged, the stress concentration phenomenon at the foot of the arch surrounded by the rock is increasing, and the structural stability of the tunnel is weakened.

4.4 Characteristics of deformation under different working conditions

Displacement is the most intuitive manifestation of rock deformation and is usually relatively large at the top and bottom of the tunnel after excavation. In this paper, the development of surrounding rock displacement for each working condition during tunnel excavation and roof loading is shown in Figure 7 (a, b, c, d, e). In Condition A, with the excavation of the tunnel, the maximum displacement of 4.3 cm occurs at the top of the right hole, which is also the maximum displacement of the surrounding rock around the tunnel. The application of the initial support (Condition B) greatly reduces the displacement value of the roof of the hole. Currently, the displacement of the roof of the right hole is 2.7cm, and the displacement of the bottom of the arch is 3.2cm. After the installation of silos and normal vehicle loading on the roof of the cave (Condition C), the displacement increases less compared to the previous stage. The

application of the mixing plant (Condition D) and concrete transportation tanker loads (Condition E) resulted in a significant increase in the tunnel load rating, resulting in a significant increase in displacement, reaching 4.7 cm at Condition E. At this displacement level, the tunnel stability is weak. Discussion on deformation characteristics and deformation control of tunnel shallow buried section

It can be seen from the results of the analysis of each working condition that the maximum displacement around the tunnel occurs at the top or bottom of the tunnel, and the displacement of the right tunnel is larger than the displacement of the left tunnel. The stress maxima are all at the foot of the arch. The range of the plastic zone in the right hole is larger than that in the left hole, and the plastic zone of peripheral rock around the tunnel without initial support appears at the position of the side wall, after the construction of the initial support, the initial support bears the lateral pressure of the peripheral rock and transfers the pressure of the peripheral rock to the foot of the tunnel initial support, and the plastic zone then transfers to the peripheral rock at the bottom of the foot of the initial support. The deformation characteristics of the shallow buried section of the tunnel under each working condition are shown in Table 3.

Condition A simulates the force on the surrounding rock when the tunnel is excavated in one go, with no additional load on the roof of the tunnel and no initial support being constructed. Under this condition, the displacement of the right tunnel roof reaches 4.3cm, which is also the maximum displacement of the surrounding rocks around the tunnel. The extreme value of the equivalent stress appeared in the region of the arch footing, which was as high as 3.74 MPa, exceeding the design value of the strength of the tunnel surrounding rock (gravel soil). Both the left and right sidewalls of the tunnel show penetrating plastic zones in the surrounding rock and the tunnel structure is extremely unstable. When the tunnel is excavated by the step or sidewall method, the tunnel structure can remain relatively stable compared to one-time excavation as stress redistribution occurs in the surrounding rock around the tunnel during tunnel excavation.

Condition B simulates the force on the surrounding rock when the initial support is constructed in time after tunnel excavation and there is no additional load on the roof of the tunnel. Under this condition, the displacement of the top of the right tunnel was 2.7cm, the displacement of the bottom of the arch was 3.2cm, and the maximum equivalent stress of 8.39MPa appeared in the foot of the arch, which was lower than the design value of the strength of the concrete of the tunnel's initial support (9.6MPa). The surrounding rock of the tunnel arch foot appears partially plastic zone, the plastic area is small, the tunnel structure is stable, but due to the structural strength of less surplus, the arch foot surrounding rock stress is more concentrated. After excavation can be used to construct the initial support, strengthen the construction quality of the initial support, construct the second lining as early as possible, and make appropriate reinforcement to the plastic region of the arch foot, or strengthen the anchoring force of the arch foot locking foot anchors, to improve the stability of the structure.

Condition C simulates the force on the surrounding rock when the initial support is constructed in time after tunnel excavation, when silos are set up at the roof of the tunnel, and when ordinary vehicle loads are applied. Under this condition, the roof displacement does not change much compared with condition B. The roof displacement, equivalent force, and plastic zone range increase only slightly, and the impact of silo and ordinary vehicle loads on the structural stability of the tunnel is relatively small.

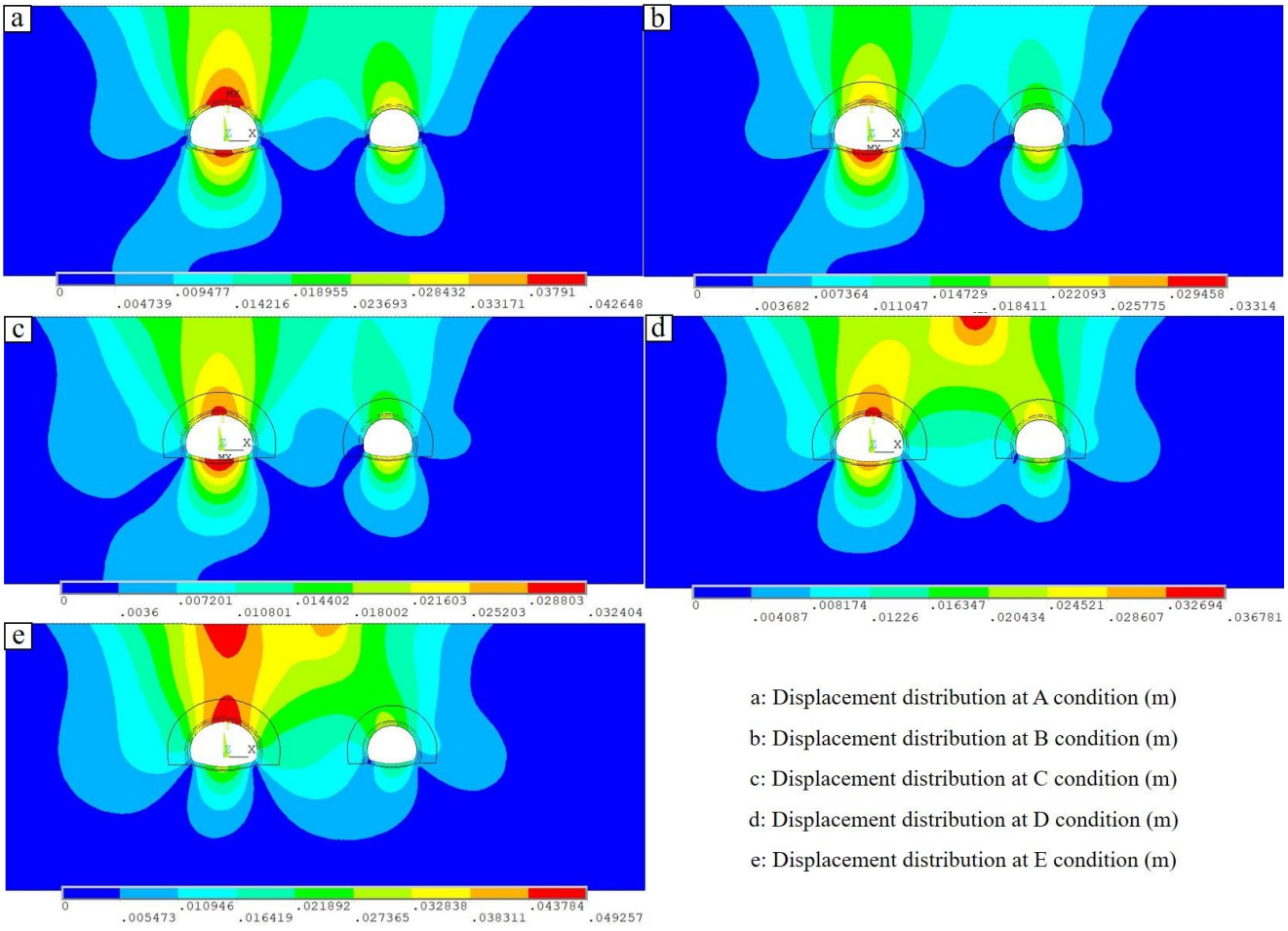

Fig.7 Displacement distribution for each working condition

Table 3 Displacement, Stress, and Plastic Strain at Critical Points of Tunnel under Different Working Conditions

Working condition	Displacement of the roof of the right hole (m)	Displacement of the roof of the left hole (m)	Von-mises stress maximum (MPa)	Maximum plastic strain	Note
A	0.043	0.031	3.74	0.012	No initial support and no load
B	0.027	0.018	8.39	0.013	With initial support and no load
C	0.028	0.019	8.42	0.014	Initial support + silo + general vehicles
D	0.033	0.027	9.09	0.015	Initial support + silo + mixing plant
E	0.047	0.029	9.59	0.02	Initial support + silo + mixing plant + concrete transportation tanker

Condition D simulates the force on the surrounding rock when the initial support is constructed promptly after tunnel excavation, when the mixing station and silo are set up at the roof of the tunnel, and when ordinary vehicle loads are applied. Under this condition, the displacement of the right tunnel roof is 3.3cm, and the maximum equivalent stress occurs in the foot of the arch area, with a maximum equivalent stress of 9.09MPa (an increase of about 9% compared with the B condition). The plastic zone of the surrounding rock at the foot of the tunnel increases to a certain extent compared to Case B, but due to less structural strength surplus and more concentrated stresses in the surrounding rock at the foot of the tunnel. The control of tunnel structural stability can be taken to strengthen the quality of overrun grouting and initial support construction, and appropriate reinforcement of the initial support at the foot of the arch to enhance the base of the foot of the arch to deal with, and at the same time, strictly implement the construction measures of the side of the excavation side of the support. Tunnel excavation immediately after the construction of the initial support, the steel frame as early as possible into the ring, strengthen the arch foot locking anchor anchors anchoring force, and timely follow-up of the second lining and backfilling of the superelevation arch, the tunnel excavation must be a completion of the second lining, the other can only be excavated, staggered construction time.

Working condition E simulates the force on the surrounding rock when the initial support is constructed in time after tunnel excavation, the mixing station is set up on the roof of the tunnel, and the concrete transportation tanker, silo, and ordinary vehicle are loaded. Under this condition, the displacement of the roof is large, the maximum value of the displacement of the roof of the right hole reaches 4.7cm, and the maximum value of the equivalent stress is as high as 9.59MPa (about 15% more than that condition B), which is equal to the design value of the strength of the concrete of the tunnel's initial support, and there is no surplus of the structural strength, and the scope of the tunnel's plastic zone and the value of the plastic strain are also increased, so that the tunnel's structural stability is weak. Therefore, when a mixing plant is set up on the roof of the tunnel, the concrete transportation tankers should be controlled to pass through the roof in a decentralized manner, and measures should be taken for working condition D to ensure the stability of the tunnel structure.

5. Conclusions

Based on the theory of elastic-plastic mechanics, this paper simulates and analyzes the stress distribution characteristics, plastic zone development, and deformation characteristics of the tunnel surrounding rock under different load combinations and summarizes the influence of load combinations on tunnel deformation and the disposal methods of surrounding rock deformation during construction. The following conclusions are drawn:

(1) In the early stage of tunnel excavation, a maximum equivalent force of 3.74 MPa was generated at the arch foot of the right tunnel, which eventually increased to 9.59 MPa with the increase of load, and this stress level is the strength limit of the initial concrete support.

(2) Tunnel excavation caused the tunnel side wall surrounding rock through the plastic zone, the initial support will be the surrounding rock pressure transfer to the tunnel arch foot, the plastic zone and then transferred to the bottom of the initial arch foot, and thereafter the increase in the load only caused by the increase in the scope of the plastic zone of the surrounding rock at the foot of the arch.

(3) At the beginning of tunnel excavation, the maximum displacement of 4.3cm occurred at the top of the right hole, and the increase of load caused the deformation of the top and bottom of the hole to increase continuously, and the maximum displacement of E condition was 4.70cm.

(4) Tunnel excavation using the step method and sidewall method can effectively reduce the stress concentration phenomenon at the arch foot. The construction measures of digging and supporting at the same time during the construction process have a positive effect on the stability of the tunnel structure.

Data Availability Statement

The original contributions presented in the study are included in the article/Supplementary Material, further inquiries can be directed to the corresponding author.

Author Contributions

Zhang Lin is responsible for all the work.

Funding

This work was supported in part by the Opening fund of State Key Laboratory of Geohazard Prevention and Geo-environment Protection (Chengdu University of Technology) (No. SKLGP2022K014), the Natural Science Foundation of Sichuan Province (No.2022NSFSC1063).

References

Adhikari Anuj Roy Nishant. (2023). Influence of Anisotropic Stress Conditions on Tunnel Deformation and Sequential Excavation Performance in Rock Mass.Journal of the Geological Society of India (7):965-974. doi: 10.1007/S12594-023-2417-7

Gao Kun,Gao Xiaogeng. (2022). Mechanical Response Analysis Due to the Influence of Particle Shape on the Stability of Sandy Ground after Tunnel Excavation[J]. Advances in Geosciences, 12(12): 1646-1659. doi: org/10.12677/AG.2022.1212160

Cao Suo,Yu Yong,Wang Bo. (2021). Viscoelasto-viscoplastic solutions for a circular tunnel based on D-P yield criterion and Nishihara model[J]. Rock and Soil Mechanics, 42(7):1925-1932. doi: 10.16285/j.rsm.2020.1637.

Giovanni Barla. (2016). Full-face excavation of large tunnels in difficult conditions. Journal of Rock Mechanics and Geotechnical Engineering, (3), 294-303. doi: 10.1016/j.jrmge.2015.12.003

Gu Jiayu. (2022). Secondary Development and Application of ANSYS Based on Rock Nonlinear Unified Elastic-plastic Model[D]. Tarim University. doi: 10.27708/d.cnki.gtlmd.2022.000409.

Gao Zhaoning, Chen Dengguo, Sun Zhenchuan, et al. (2020). Stability analysis of tunnel surrounding rock considering influence of damage anddilatancy[J]. China Safety Science Journal, 30(7): 159-165.doi: 10.16265/j.cnki.issn1003-3033.2020.07.024.

Guo Xiaolong, Tan Zhongsheng; Yu Yu. (2022). Study on Large Deformation Control Technology and Deformation ControlCriteria for Soft Rock Tunnels of Chengdu-Lanzhou Railway[J]. Journal of the China Railway Society, 44(03): 86-104.

Jiang Pingwei, Zhang Zhihong, Zheng Hong Huang Jinkun. (2024). Coupling analysis method of grouting construction with deformation response of adjacent existing tunnel. Underground Space: 312-330. doi: 10.1016/J.UNDSP.2023.07.005

Jiang Han, Fang Xiaolong, Yu Ming,Li Lin,Han Bing,Gao Song et al. (2023). Study on the construction deformation of a slotted shield in loess tunnels with different buried depths and large sections. Frontiers in Earth Science. doi: 10.3389/FEART.2022.1075928

LIU Haiting. (2022). Study on dynamic response characteristics and stability control of carbonaceous shale high-speed railway tunnel under train load[D]. Shandong University. doi: 10.27272/d.cnki.gshdu.2022.001156

Lunardi P. (2008). Design and construction of tunnels:the analysis of controlled deformation in rocks and soils[M].Berlin Heidelberg:Springer.

Tang Xi. (2023). Influence analysis on underground excavation of subway tunnels undercrossing elevated section of existing lines[J]. Building Structure, 53(09):141-146+152. doi: 10.19701/j.jzjg.20222652

Wang Jinming,Yang Xiaoli. (2008). Influence of Different Construction Methods on Ground Settlement for Shallow Metro Tunnel by Excavation[J]. Journal of Shihezi University (Natural Science). 4: 499-503. doi: 10.13880/j.cnki.65-1174/n.2008.04.011

Wang Junxiang, Jiang Annan. (2015). An elastoplastic damage constitutive model of rock and its application to tunnel engineering[J]. Rock and Soil Mechanics, 36(04):1147-1158. doi: 10.16285/j.rsm.2015.04.032

Wang Junxiang. (2014). Study on Elastoplastic Damage and MHC Coupling Model ofRock and Numerical Algorithm[D]. Dalian Maritime University.

Xu Ying,Yu Yuchao,Yao Wei,Xia Kaiwen,Tang Junxi & Zhan Zhifeng.(2023).Dynamic failure characteristics of surrounding rocks under different lateral pressure coefficients in deep tunnel transient excavation.. Geomechanics and geophysics for geo-energy and geo-resources (1),17-17. doi: 10.1007/S40948-023-00563-X

Xu Xiaoding,Zhou Yuejin,Zhu Chun,Zeng Chunlin & Guo Chong. (2022). An Analytical Model for the Excavation Damage Zone in Tunnel Surrounding Rock. Minerals (10),1321-1321. doi: 10.3390/MIN12101321

Zgur S, Tamer T. (2021). Assessment of damage zone thickness and wall convergence for tunnels excavated in strain-softening rock masses[J]. Tunnelling and Underground Space Technology, 108:103722. doi: 10.1016/j.tust.2020.103722

Zhang Xingwei, Wang Chao. (2022). Analysis of the Stability of Tunnel Surrounding Rock and Ground Settlement in Soft Layered Foundation[J]. Chinese Journal of Underground Space and Engineering. 18(A1): 396-403, 411.

Zhu Yiqiao. (2022). Analysis of the influence of large deep foundation pit excavation on nearby metro shield tunnel[J]. Building Structure, 52(S1): 2561-2567. doi: 10.26914/c.cnkihy.2022.086557

Zhang Fan, Sheng Qian, Zhu Zeqi, et al. (2008). Study on post-peak mechanical behavior and starain-softeningmodel of three gorges granite[J]. Chinese Journal of Rock Mechanics and Engineering, 27:2651-2655.

Zhang Guohua, Zhang Bowen, Tan Fei, Liu Zhonghou, Zou Junpeng, Xie Zhongzhi. et al. (2023). Origin of clay in granite intrusive contact zone and its influence on tunnel deformation and instability.Engineering Geology. doi: 10.1016/J.ENGGEO.2022.106965